

General Relativistic Force-Free Electrodynamics: A New Code and Applications to Black Hole Magnetospheres

Jonathan C. McKinney^{*}

Institute for Theory and Computation, Harvard-Smithsonian Center for Astrophysics, 60 Garden Street, MS 51, Cambridge, MA 02138, USA

Accepted 2006 January 18. Received 2005 Dec 8; in original form 2005 Dec 8

ABSTRACT

The force-free limit of magnetohydrodynamics (MHD) is often a reasonable approximation to model black hole and neutron star magnetospheres. We describe a general relativistic force-free (GRFFE) formulation that allows general relativistic magnetohydrodynamic (GRMHD) codes to directly evolve the GRFFE equations of motion. Established, accurate, and well-tested conservative GRMHD codes can simply add a new inversion piece of code to their existing code, while continuing to use all the already-developed facilities present in their GRMHD code. We show how to enforce the $\mathbf{E} \cdot \mathbf{B} = 0$ constraint and energy conservation, and we introduce a simplified general model of the dissipation of the electric field to enforce the $B^2 - E^2 > 0$ constraint. We also introduce a simplified yet general method to resolve current sheets, without much reconnection, over many dynamical times. This formulation is incorporated into an existing GRMHD code (HARM), which is demonstrated to give accurate and robust GRFFE results for Minkowski and black hole space-times.

Key words: black hole physics, galaxies: jets, gamma rays: bursts, MHD, stars: neutron, magnetic field, outflows, methods: numerical

1 INTRODUCTION

General relativistic force-free electrodynamics (GRFFE) is the low-inertia limit of general relativistic magnetohydrodynamics (GRMHD) (see, e.g., Komissarov 2002b, 2004a). Neutron star and black hole magnetospheres exhibit regions of space that are very nearly force-free, and self-consistent moderately realistic quasi-analytic solutions exist that describe the ideal MHD or force-free environment of such systems (see, e.g., Blandford & Znajek 1977; Contopoulos et al. 1999; Goodwin et al. 2004; Beskin & Nokhrina 2005; Gruzinov 2005). It is generally difficult to solve the GRFFE equations to find even stationary solutions, except with simplified assumptions, that apply to astrophysical systems. For example, despite recent progress in studies of neutron star magnetospheres, no self-consistent analytic solution considers general relativistic effects. Also, the solution of Blandford & Znajek (1977) is the only self-consistent analytic force-free solution that has a realistic Poynting jet. Also, analytic solutions typically assume stationarity and axisymmetry and so rarely address the global or local stability of the solutions against time-dependent or nonaxisym-

metric modes or stability against reconnection in current sheets if present.

One simple technique to seek stationary solutions and to study time-dependent stability is to directly numerically integrate the GRFFE equations of motion. Both the GRMHD and GRFFE equations of motion can be written as a set of conservation laws that can be directly integrated. Conservative numerical GRMHD methods, such as of HARM (Gammie et al. 2003a), use so-called “primitive” quantities (\mathbf{P}) to define so-called “conserved” quantities (\mathbf{U}), fluxes (\mathbf{F}), and source (\mathbf{S}) terms. The temporal integration is determined by solving the set of “conservation” equations, which can be written as

$$\frac{\partial U^p(\mathbf{P})}{\partial t} = -\frac{\partial F^{pi}(\mathbf{P})}{\partial x^i} + S^p(\mathbf{P}), \quad (1)$$

where p labels the conservation equation and i is the spatial index. The set of source terms (S^p) accounts for the connection coefficients or other sources of mass-energy-momentum. Thus conservation is explicitly true as long as the source terms vanish. For an axisymmetric, stationary metric and as written in HARM, energy and angular momentum are explicitly conserved to machine error because the source terms vanish. HARM has been successfully used to study black hole accretion flows, winds, and Poynting

^{*} E-mail: jmckinney@cfa.harvard.edu

jets (Gammie et al. 2003a; Gammie, Shapiro, & McKinney 2004; McKinney & Gammie 2004; McKinney 2005a,b,c).

While GRFFE is mathematically just the no-inertia limit of GRMHD, numerical truncation errors limit the use of GRMHD codes in evolving systems with regions where the magnetic energy density greatly exceeds the rest-mass energy (see, e.g., McKinney & Gammie 2004; Komissarov 2004b, 2005a,b). Conversely, the GRFFE equations of motion do not describe the rest-mass motion along field lines or the thermal energy of the particles. So long as the inertia of particles remains negligible, the GRFFE equations of motion properly describe the magnetic field geometry and motion.

A GRFFE code can be used to study neutron star and black hole magnetospheres. For example, the origin of the collimation and stability of astrophysical jets remains unexplained. A GRFFE code can be used to examine the origin of the collimation and the stability of any model for a Poynting-dominated jet.

Existing jet solutions may not be stable and self-collimation of isolated jets may not work (Spruit 1996; Okamoto 1999, 2000, 2003). Collimation by a predominately toroidal field (hoop stress) may lead to a pinch/kink instability, whereas poloidal collimation works only if the jet is surrounded by an extended disk wind (Spruit 1996; Begelman & Li 1994; Begelman 1998). The solution to the collimation problem may be that the disk wind collimates the Poynting jet. By using both GRMHD and GRFFE numerical models, the origin of collimation, acceleration, and stability of jets can be examined. Thus it is more efficient to have a single code be able to perform both GRMHD and GRFFE studies.

Even a black hole system accreting a thick disk has a force-free magnetosphere (McKinney & Gammie 2004). Such a magnetosphere quantitatively agrees with the solution by Blandford & Znajek (1977) for low black hole spins and agrees qualitatively for high spins (McKinney & Gammie 2004; Komissarov 2004b, 2005a). Gamma-ray bursts (GRBs), active galactic nuclei (AGN), and x-ray binaries probably exhibit both a Poynting-dominated jet and a jet from the disk, as suggested by GRMHD numerical models (McKinney 2005b,c). In particular, of all jet mechanisms, the Blandford-Znajek driven jet is the only one that can clearly produce an ultrarelativistic jet (McKinney 2005a). Thus it is important to study the Blandford-Znajek process in detail. A GRFFE code can help determine the stability of the Poynting-dominated jet generated by the Blandford-Znajek effect. For example, a GRFFE code was used to study the pure monopole version of the Blandford-Znajek solution, which is found to be stable (Komissarov 2001, 2002a). However, general Poynting-dominated jets produced by the Blandford-Znajek effect may be violently unstable to pinch and kink instabilities (see, e.g., Li 2000, but see also Tomimatsu et al. 2001). A GRFFE code proves valuable in stability analyses by avoiding the difficulty of analytically crossing the light cylinder (see, e.g., Tomimatsu et al. 2001), which manifests itself as a singularity in the Grad-Shafranov equation for stationary solutions.

The goal of this paper is to formulate the GRFFE equations of motion such that a conservative GRMHD code can be used with small modifications. Present numerical meth-

ods directly evolve the electric and magnetic fields (primitive quantities are $\{\mathbf{E}, \mathbf{B}\}$, the field-evolution approach) and have to explicitly check that the velocity is less than the speed of light (i.e. magnetic energy density is greater than electric energy density, $B^2 - E^2 > 0$) since the electric and magnetic field are evolved with no constraint on their evolution (Komissarov 2002b; Krasnopolsky et al. 2005). The method we describe evolves the drift velocity and magnetic field (primitive quantities are $\{\mathbf{v}, \mathbf{B}\}$, (velocity-evolution approach), explicitly breaks down when that constraint is violated and this ensures a physical and causal evolution.

We show that this velocity-evolution approach can be directly used by GRMHD codes, and explicitly discuss how this is done for conservative numerical methods. Many GRMHD codes have recently been developed (Koide et al. 1999; Komissarov 1999; Gammie et al. 2003a; De Villiers & Hawley 2003; Shibata & Sekiguchi 2005; Anninos et al. 2005; Anton et al. 2005). Our discussion applies to any GRMHD method, but focuses on conservative-based codes. We show that a separate GRFFE code does not have to be developed, and many of the tools and methods used to make the GRMHD code perform well carry directly over to the GRFFE version.

§ 2 shows how a conservative GRMHD code can be used to evolve the GRFFE equations of motion. Simplified models of dissipation in GRFFE are discussed in order to handle regions here the electric field dominates the magnetic field.

§ 3 includes a series of standard tests of the GRFFE code.

§ 4 discusses models of black hole magnetospheres. This section demonstrates the usefulness of the GRFFE equations of motion and the model of dissipation.

§ 5 summarizes the results of the paper.

The GRMHD notation follows Misner et al. (1973) and we use Heaviside-Lorentz units unless otherwise specified, which is like Gaussian units without the 4π . For example, the 4-velocity components are u^μ (contravariant) or u_μ (covariant). For a black hole with angular momentum $J = jGM^2/c$, $j = a/M$ is the dimensionless Kerr parameter with $-1 \leq j \leq 1$. The contravariant metric components are $g^{\mu\nu}$ and covariant components are $g_{\mu\nu}$. The comoving energy density is $b^2/2$, where b^μ is the comoving magnetic field. See Gammie et al. (2003a); McKinney & Gammie (2004) for details.

2 FORCE-FREE ELECTRODYNAMICS

This section shows how a conservative-based algorithm designed for solving the ideal GRMHD equations of motion based upon the velocity and a magnetic field can be used to solve the GRFFE equations of motion. In particular, the electric and magnetic field are used to derive the velocity of the frame in which the electric field vanishes. This allows a conservative ideal GRMHD numerical code to evolve the force-free equations of motion by simply modifying the inversion from conserved quantities to primitive quantities.

The force-free electrodynamics equations of motion are the 8 Maxwell equations:

$$\nabla_\mu F^{\mu\nu} = -J^\nu, \quad (2)$$

where $F^{\mu\nu}$ are the components of the Faraday tensor and J^μ are the components of the current density, and

$$\nabla_\mu {}^*F^{\mu\nu} = 0, \quad (3)$$

where ${}^*F^{\mu\nu} \equiv \frac{1}{2}\epsilon^{\mu\nu\alpha\beta}F_{\alpha\beta}$ are the components of the dual Faraday (or Maxwell) tensor, $F^{\mu\nu} \equiv -\frac{1}{2}\epsilon^{\mu\nu\alpha\beta}{}^*F_{\alpha\beta}$, $\epsilon^{\alpha\beta\delta\gamma} \equiv (-1/\sqrt{-g})[\alpha\beta\gamma\delta]$, and $\epsilon_{\alpha\beta\delta\gamma} \equiv \sqrt{-g}[\alpha\beta\gamma\delta]$, where brackets denote the unit length completely antisymmetric tensor. These 8 equations define 6 evolution equations and 2 differential constraints.

By the antisymmetry and duality of the Faraday and Maxwell tensors, they be expressed in component form as

$$F^{\alpha\beta} \equiv f\eta^\alpha E^\beta - f\eta^\beta E^\alpha - hB_\gamma\eta_\delta\epsilon^{\alpha\beta\gamma\delta} \quad (4)$$

and

$${}^*F^{\alpha\beta} \equiv -h\eta^\alpha B^\beta + h\eta^\beta B^\alpha - fE_\gamma\eta_\delta\epsilon^{\alpha\beta\gamma\delta}, \quad (5)$$

where f and h are arbitrary independent constants that we set to be $f = h = 1$ consistent with the conventions in Misner et al. (1973), and see also, e.g., Baumgarte & Shapiro (2003). Here $E^\alpha \equiv \eta_\beta F^{\alpha\beta}$, $B^\alpha \equiv \eta_\beta {}^*F^{\beta\alpha}$, and η^μ is an arbitrary 4-vector. This gives that $F_{\mu\nu}{}^*F^{\mu\nu} = 4E^\mu B_\mu(-\eta^2)$ and $F^{\mu\nu}F_{\mu\nu} = 2(B^2 - E^2)(-\eta^2)$. For a time-like η^μ , the sign conventions are as in special relativity.

The electromagnetic stress energy tensor is constructed from the Faraday tensor and must be quadratic in the field strengths, symmetric, and is divergenceless in vacuum by Maxwell's equations. This unique tensor is

$$T^{\mu\nu} = F^\mu{}_\lambda F^{\nu\lambda} - \frac{1}{4}g^{\mu\nu}F^{\lambda\kappa}F_{\lambda\kappa}, \quad (6)$$

where $g^{\mu\nu}$ are the components of the metric. The duality between the Faraday and Maxwell tensors and the definitions of E^μ and B^μ give that

$$\begin{aligned} T^{\mu\nu} &= \left(\frac{B^2 + E^2}{2}\right)(\eta^\mu\eta^\nu + P^{\mu\nu}) \\ &- (-\eta^2)(B^\mu B^\nu + E^\mu E^\nu) \\ &- \eta_\alpha E_\beta B_\kappa \left(\eta^\mu \epsilon^{\nu\alpha\beta\kappa} + \eta^\nu \epsilon^{\mu\alpha\beta\kappa}\right), \end{aligned} \quad (7)$$

where the projection operator $P^{\mu\nu} = (-\eta^2)g^{\mu\nu} + \eta^\mu\eta^\nu$. For example, the energy density in frame η^μ is $\eta_\mu\eta_\nu T^{\mu\nu} = \eta^4(E^2 + B^2)/2$, which for a time-like η^μ is the same expression as in special relativity. If the electromagnetic field is the only source of stress-energy, then equations (2) are equivalent to the energy-momentum conservation equations

$$\nabla_\mu T^{\mu\nu} = J_\mu F^{\mu\nu} = 0, \quad (8)$$

where only 2 of the 4 components of equation (8) are independent because equations (8) implies

$$F_{\mu\nu}{}^*F^{\mu\nu} = 4E^\mu B_\mu(-\eta^2) = 0. \quad (9)$$

For more details see Komissarov (2002b, 2004a).

2.1 Inversion

Conservative numerical GRMHD methods, such as of HARM, operate primarily on so-called ‘‘primitive’’ quantities (\mathbf{P}): fluid density, fluid internal energy, coordinate fluid velocity, and the lab-frame coordinate magnetic field.

HARM uses the primitive quantities to define so-called ‘‘conserved’’ quantities (\mathbf{U}) and the fluxes (\mathbf{F}), which are both closed-form operations. These conserved quantities can be evolved forward in time, but then an inversion to primitive quantities is required to easily define the fluxes and other required quantities to determine the next update.

No closed form solution appears to exist in GRMHD, so most inversion methods rely on iterative procedures such as Newton's method. This approach can be used in force-free electrodynamics, but may not always work due to known problems (such as poorly conditioned or singular Jacobians) with Newton's method. However, a closed-form solution does exist for force-free electrodynamics, as described below.

The only conserved quantities of relevance in force-free electrodynamics are the lab-frame momentums T_μ^t (the energy evolution equation giving the $\mu = t$ term is actually redundant) and the lab-frame magnetic field B^μ (only 3 components are independent). If one could obtain E^μ , then one could reconstruct the Faraday from equation (4) or any other quantities from E^μ and B^μ . It is straight-forward to show that if $E^\alpha B_\alpha = 0$, then

$$E^\alpha = \epsilon^{\alpha\beta\gamma\delta} B_\beta T_\gamma^\xi \eta_\xi / (B^2 \eta^4), \quad (10)$$

as shown by a substitution of equation (6) and equation (4) into this expression. Only the spatial components of $\eta_\mu T_\nu^\mu$ and B^μ are needed if one chooses a special form of η^μ . Notice that $E^\alpha B_\alpha = 0$ is explicitly true, therefore the degeneracy condition of $\mathbf{E} \cdot \mathbf{B} = 0$ can be preserved to machine error regardless of the truncation error in \mathbf{T} or \mathbf{B} . Also notice that equation (10) projects out a component perpendicular to time, the spatial field, and the momentums. For a fixed field B^i , only 2 components of the electric field are independent.

One may choose to have $\eta^2 = -1$ such that η^μ only depends on the metric. One choice is $\eta_\mu = \{-\alpha, 0, 0, 0\}$, where $\alpha \equiv 1/\sqrt{-g^{tt}}$. Then $\eta^\mu = (1/\alpha)\{1, -\beta^i\}$, where $\beta^i \equiv \alpha^2 g^{ti}$. This defines a zero angular momentum (ZAMO) frame. This choice of η^μ makes it possible to only require T_i^t and B^i to obtain E^α in equation (10).

Another interesting choice for η^μ is to have $E^\nu \equiv \eta_\mu F^{\mu\nu} = 0$. In the ideal GRMHD equations of motion, for a fluid velocity u^μ , this choice corresponds to the electric field in the comoving frame u^μ being $e^\nu \equiv u_\mu F^{\mu\nu} = 0$. Then $\eta^2 = -1$ since the fluid velocity is time-like. In force-free electrodynamics, there is no unique 4-velocity that satisfies $e^\nu = 0$, but one such frame is constructed below that is uniquely always time-like with a minimum Lorentz factor with respect to the frame with 4-velocity η^μ .

As shown next, any two frames with 4-velocities u^μ and η^μ can be easily related to determine a 4-velocity of the frame in which $e^\nu = 0$ for the Faraday defined in terms of η^μ . Thus the metric and Faraday alone determine a 4-velocity that allows one to use the ideal GRMHD Faraday,

$$F^{\alpha\beta} \equiv -b_\gamma u_\delta \epsilon^{\alpha\beta\gamma\delta} \quad (11)$$

and Maxwell,

$${}^*F^{\alpha\beta} \equiv -u^\alpha b^\beta + u^\beta b^\alpha, \quad (12)$$

where $b^\nu \equiv u_\mu {}^*F^{\mu\nu}$. This formulation and sign conventions are the same as used in HARM. In HARM, a new 4-velocity is introduced that is unique by being related to a physical observer for any space-time and has well-behaved interpolated values,

$$\tilde{u}^i \equiv u^i - \gamma \eta^i, \quad (13)$$

where $\gamma = -u^\alpha \eta_\alpha$ and so $u^t = \gamma/\alpha$. This additional term represents the spatial drift of the ZAMO frame defined earlier. One can show that $\gamma = (1 + q^2)^{1/2}$ with $q^2 \equiv g_{ij} \tilde{u}^i \tilde{u}^j$.

To obtain the 4-velocity, notice that

$$0 = e^\alpha = -(v_\beta E^\beta) \eta^\alpha + E^\alpha + v_\beta B_\gamma \eta_\delta \epsilon^{\alpha\beta\gamma\delta}, \quad (14)$$

where $v_\beta \equiv -u_\beta/(u^\alpha \eta_\alpha)$. The most general form of the 4-velocity that satisfies the above is

$$v_\beta = G \left(\frac{-\epsilon_{\beta\sigma\epsilon\eta} \eta^\sigma E^\epsilon B^\eta}{-\eta^2 B^2} \right) + H \left(\frac{\eta_\beta}{-\eta^2} \right) + K \left(\frac{E_\beta}{\sqrt{-\eta^2 E^2}} \right) + L \left(\frac{B_\beta}{\sqrt{-\eta^2 B^2}} \right), \quad (15)$$

where G , H , K , and L are functions to be determined. Each term represents one of four orthogonal directions, and when multiplied by arbitrary functions represent the most general solution. The only nontrivial term is the antisymmetric product between the last term in equation (14) and the first term in equation (15). Substitution of this v^β into equation (14) gives that $G = 1$. Since $v_\beta \eta^\beta = -1$, then $H = 1$. With $u_\beta = \gamma v_\beta$, then $u^2 = -1$ gives that $\gamma = \sqrt{-\eta^2 B^2 / ((1 - K^2) B^2 - E^2)}$, which simply defines $\gamma = -u^\alpha \eta_\alpha$ as the Lorentz factor between the two frames. All terms proportional to K are orthogonal to each other and to E^α , and so in general $K = 0$. Hence, $u^\alpha E_\alpha = 0$. To determine L , notice that b^α in $F^{\mu\nu}$ in equation (12) can be written as

$$b^\alpha = \frac{P_\beta^\alpha B^\beta}{\gamma}, \quad (16)$$

where $P_\beta^\alpha = \delta_\beta^\alpha + u^\alpha u_\beta$ is the projection tensor. Thus b^α has terms proportional to B^α and u^α . So extra terms added to u^α proportional to B^α vanish due to the antisymmetry of the Maxwell and so do not contribute to the stress-energy tensor or the equations of motion. Thus, the function L parameterizes the arbitrary velocity component along a field line, and we choose $L = 0$ to minimize the Lorentz factor of the frame. Hence, $u^\alpha B_\alpha = 0$ and so $b^\alpha = B^\alpha/\gamma$. With this choice of L , if $B^2 - E^2 > 0$, then the frame with u^μ is always time-like. Thus the frame defined by the 4-velocity

$$u^\alpha = \left(\sqrt{\frac{B^2}{B^2 - E^2}} \right) \left(\eta^\alpha - \frac{\epsilon^{\alpha\beta\gamma\delta} \eta_\beta E_\gamma B_\delta}{B^2} \right) \quad (17)$$

is time-like for any force-free electrodynamic solution. Thus, by construction, we have shown that in force-free electrodynamics that it is possible to boost into a time-like frame where the electric field vanishes and thus the Poynting flux vanishes (see also, e.g. Komissarov 2002b). This also shows that force-free electrodynamics is a causal limit of GRMHD as long as $B^2 - E^2 > 0$. This 4-velocity also represents a unique covariant definition of the ‘‘field-line velocity,’’ and also describes the field-line velocity even in ideal MHD.

A GRMHD code may only need the coordinate lab-frame 3-velocity. Since $u^t = \gamma \eta^t$, then for the earlier defined ZAMO frame η^μ , the coordinate lab-frame 3-velocity is given by

$$v^i \equiv \frac{u^i}{u^t} = -\beta^i + \alpha^2 \frac{[ijk] E_j B_k}{\sqrt{-g} B^2} \quad (18)$$

The second term in equation (17) represents the purely spatial ‘‘ $\mathbf{E} \times \mathbf{B}$ drift.’’ Note that there is no evolutionary constraint on $T^{\mu\nu}$ that forces $B^2 - E^2 > 0$, and when this is violated the force-free model is no longer physical. The value of v^ϕ coincides with the ‘‘field rotation frequency’’ $\Omega_F = F_{tr}/F_{r\phi} = F_{t\theta}/F_{\theta\phi}$ for stationary axisymmetric flows for which $v^r = v^\theta = 0$.

Now the inversion from $\{T_i^t, B^i\} \rightarrow \{E^i, B^i\}$ and then $\rightarrow \{v^i, B^i\}$ completely defines equations (11) and (12) for a general relativistic force-free electrodynamics evolution using a conservative GRMHD code.

Obviously this formulation can be also used to study special relativistic models as well. Notice that in special relativity that the derived velocity expression reduces to the so-called ‘‘electromagnetic 3-velocity’’ $\mathbf{v} = \mathbf{E} \times \mathbf{B}/B^2 = \mathbf{S}/B^2$, where $\mathbf{S} = \mathbf{E} \times \mathbf{B}$ is the Poynting flux.

As used in HARM, this formulation preserves $\nabla \cdot \mathbf{B} = 0$ and $\mathbf{E} \cdot \mathbf{B} = 0$ to round-off error for both the GRMHD and GRFFE equations of motion. Notice that this differs from other formulations that only preserve $\nabla \cdot \mathbf{B} = 0$ and $\mathbf{E} \cdot \mathbf{B} = 0$ to truncation error (Komissarov 2002b, 2004a)

The fact that the field-evolution approach does not break down might be considered an advantage when seeking stationary solutions. In such a case the evolution may have regions that only transiently have $B^2 - E^2 < 0$ and the integration can pass smoothly through this region into a physical solution space. A related advantage of the field-evolution approach is that Runge-Kutta temporal evolution can recover the correct temporal order of accuracy. That is, without characteristic interpolation, HARM uses Runge-Kutta to time step to achieve higher order temporal accuracy. Runge-Kutta is only first order accurate for the first substep, but after all substeps are completed, the method is accurate to arbitrary order. The velocity-evolution approach can yield an unphysical result for a substep and be unable to continue or treat the result as a violation of force-free electrodynamics, while the field-evolution approach can avoid such first order errors and recover to arbitrary order accuracy. However, we have found the velocity-evolution approach to be sufficient. This issue of falling outside the light cone is the same issue one encounters when evolving the GRMHD equations of motion, and in that case the author knows of no method that does not require the velocity at some point during the integration, so the issue is treated as a generic one that simply requires a more accurate integration.

2.2 Currents

This section shows that the currents can be computed without time derivatives, which is numerically convenient to avoid storing data at previous times. In ideal MHD or force-free electrodynamics there are many dependent ways of equally describing the same physics. Researchers often invoke, such as in discussions of current closure, the current and the magnetic field as a more intuitive set of quantities than the electromagnetic fields. The current could be computed from

$$J^\alpha \equiv F_{;\beta}^{\alpha\beta}, \quad (19)$$

which apparently requires time derivatives. In force-free electrodynamics, however, the current (like the 4-velocity) sits

in the null space of $F^{\alpha\beta}$, i.e. $J^\alpha F_\alpha^\beta = 0$. Hence, $J^\alpha E_\alpha = 0$. The same analysis as in section 2.1 leads to the same result for J^α except the function L is no longer arbitrary, where here

$$L = \left(\frac{J_\beta B^\beta}{\rho_{q,\eta}} \right) \left(\sqrt{\frac{-\eta^2}{B^2}} \right), \quad (20)$$

where $\rho_{q,\eta} \equiv J^\alpha \eta_\alpha$, which only actually requires spatial derivatives if $\eta_\mu = \{-\alpha, 0, 0, 0\}$. Plugging equations (4) into equations (19) and contracting J_β with B^β gives

$$J_\beta B^\beta = B^\beta \left(E^\alpha \eta_{\beta;\alpha} - \eta^\alpha E_{\beta;\alpha} - (B_\gamma \eta_\delta \epsilon^{\beta\alpha\gamma\delta})_{;\alpha} \right), \quad (21)$$

where the first and last terms only require spatial derivatives with the chosen η_μ . Using

$${}^*F_{;\beta}^{\alpha\beta} = 0, \quad (22)$$

and contracting with E_α , the second term in equation (21) can be written as

$$-B^\beta \eta^\alpha E_{\beta;\alpha} = B^\alpha E^\beta \eta_{\beta;\alpha} - E_{\beta;\alpha} E_\gamma \eta_\delta \epsilon^{\beta\alpha\gamma\delta}. \quad (23)$$

Now, for the chosen η_μ , each term in equation (21) only requires spatial derivatives. So the current can be written, only actually requiring spatial derivatives, as

$$J^\alpha = \rho_{q,\eta} \left(\eta^\alpha - \frac{\epsilon^{\alpha\beta\gamma\delta} \eta_\beta E_\gamma B_\delta}{B^2} \right) + B^\alpha \left(\frac{J^\beta B_\beta}{B^2} \right), \quad (24)$$

where finally

$$J^\beta B_\beta = E^\alpha B^\beta (\eta_{\beta;\alpha} + \eta_{\alpha;\beta}) + (B_{\alpha;\beta} B_\gamma - E_{\alpha;\beta} E_\gamma) (\eta_\delta \epsilon^{\alpha\beta\gamma\delta}), \quad (25)$$

where the asymmetry between E^α and B^α just expresses the asymmetry in Maxwell's equations for J^α . One can use equation (17) to write

$$J^\alpha = u^\alpha \left(\frac{\rho_{q,\eta}}{\gamma} \right) + B^\alpha \left(\frac{J^\beta B_\beta}{B^2} \right). \quad (26)$$

That is, there is a perpendicular drift current (J_\perp) and a field-aligned current (J_\parallel), i.e.

$$J^\alpha = J_\perp^\alpha + J_\parallel^\alpha. \quad (27)$$

Equation (26) is Ohm's law in dissipationless GRFFE. In the special relativistic regime this reduces to a lab-frame current density of

$$\mathbf{J} = \frac{\mathbf{E} \times \mathbf{B} (\nabla \cdot \mathbf{E}) + \mathbf{B} (\mathbf{B} \cdot (\nabla \times \mathbf{B}) - \mathbf{E} \cdot (\nabla \times \mathbf{E}))}{B^2}, \quad (28)$$

where $\eta_\alpha J^\alpha = \rho_{q,\eta} = -\alpha J^t = -\nabla \cdot \mathbf{E}$ is the charge density in the frame moving with 4-velocity η^μ . As in general, the special relativistic equation obviously has no time derivatives.

2.3 Jump Conditions

Conservative schemes are often based upon 1D piece-wise constant Godunov methods that achieve higher than first order accuracy by relying on a one-dimensional interpolation from, e.g., grid cell centers to cell interfaces. The interpolated states are assumed to be approximately constant over the cell face, otherwise a generalized Riemann problem must be solved (see, e.g. Toro 1999). The 1D Godunov scheme

then explicitly treats the cell interface discontinuity appropriately and reduces to a trivial form for smooth flows. However, while the hydrodynamic equations of motion allow arbitrary left and right initial states, the electromagnetic field must obey general well-known jump conditions as a manifestation of the Bianchi identities and the antisymmetry of the Faraday tensor (see, e.g., chpt. 15 of Misner et al. 1973). Alternatively stated, electrodynamics can be written as a set of Hamilton-Jacobi equations involving the vector potential and the electric field. Arbitrary interpolation of arbitrary quantities does not generally enforce these jump conditions. Thus, these jump conditions must be self-consistently enforced by interpolating appropriate quantities in the appropriate way.

HARM directly operates on the magnetic field rather than the magnetic vector potential, so the scheme must enforce the electrodynamic jump conditions on the electric and magnetic fields. For schemes that only interpolate in space and not time, one only requires the spatial jump conditions. The jump conditions across a one-dimensional space-like surface for a single lab-frame time (t) are obtained by integrating Maxwell's equations. For simplicity define $\sqrt{-g} \tilde{E}_\alpha \equiv t^\beta F_{\alpha\beta}$ and $\sqrt{-g} \tilde{B}_\alpha \equiv t^\beta {}^*F_{\beta\alpha}$. Also, consider three arbitrary orthogonal space-like vectors A, B, C that describe a space-like volume and the time-like (often but not always Killing) vector $t^\alpha = \{1, 0, 0, 0\}$. For the homogeneous Maxwell equations,

$$0 = \int \frac{(\sqrt{-g} F^{\mu\nu})_{;\nu}}{\sqrt{-g}} d\Sigma_\mu, \quad (29)$$

where ${}^*F^{ij} = [ijk] \tilde{E}_k$. First, let $d\Sigma_\mu = \epsilon_{\mu\alpha\beta\gamma} t^\alpha dA^\beta dB^\gamma$ be a 1-form 2-volume for a single lab-frame time (see, e.g., Lichnerowicz 1967, 1976; Anile 1989). Then equation (29) gives for the two spatial parallel components that

$$\Delta_C \int \sqrt{-g} \tilde{E}_A d_A [CAB] = 0, \quad (30)$$

where the C -direction is chosen as perpendicular to the surface and never is a sum implied for $[CAB]$, which only gives the 3-signature for arbitrary, but fixed, A, B, C corresponding to any 3 spatial directions. Choosing instead $d\Sigma_\mu = \epsilon_{\mu\alpha\beta\gamma} dA^\alpha dB^\beta dC^\gamma$, one has for the contravariant field that

$$\Delta_C \int \sqrt{-g} B^C dA dB = 0. \quad (31)$$

Likewise, for the inhomogeneous Maxwell equations,

$$\int J^\mu d\Sigma_\mu = \int \frac{(\sqrt{-g} F^{\mu\nu})_{;\nu}}{\sqrt{-g}} d\Sigma_\mu, \quad (32)$$

where $F^{ij} = [ijk] \tilde{B}_k$. With $d\Sigma_\mu = \epsilon_{\mu\alpha\beta\gamma} t^\alpha dA^\beta dB^\gamma$, then

$$\Delta_C \int \sqrt{-g} \tilde{B}_A dA = [CAB] \int \sqrt{-g} J^B dAdC, \quad (33)$$

for a possible surface current $J^B \equiv \delta(C) K^B$, where upper (lower) A, B, C denotes the contravariant (covariant) components parallel to the surface. Choosing instead $d\Sigma_\mu = \epsilon_{\mu\alpha\beta\gamma} dA^\alpha dB^\beta dC^\gamma$ for space-like orthogonal A, B , and C , one has for the contravariant field that

$$\Delta_C \int \sqrt{-g} E^C dA dB = \int \eta_\mu J^\mu \sqrt{-g} dAdBdC, \quad (34)$$

for a possible surface charge $\rho_{q,\eta} = \eta_\mu J^\mu \equiv \delta(C)\sigma_{q,\eta}$, where $\sigma_{q,\eta}$ is the surface charge in the frame moving with 4-velocity η^μ and the C -direction is taken to be across the surface.

For an infinitesimal surface $\sqrt{-g}dAdB$, lengths $\sqrt{-g}dA$ and $\sqrt{-g}dB$, or for point values of the fields, these expressions reduce to

$$\Delta_C \tilde{E}_A [CAB] = 0, \quad (35)$$

$$\Delta_C B^C = 0, \quad (36)$$

and

$$\Delta_C \tilde{B}_A = [CAB]K^B, \quad (37)$$

$$\Delta_C E^C = \sigma_{q,\eta}, \quad (38)$$

which apart from the concern with $\sqrt{-g}$, the contravariant vs. covariant components, and \tilde{E}, \tilde{B} vs. E, B is identical to the Cartesian special relativistic expressions for the jump conditions. Notice that no distinction is made between bound and free charges or currents, so these expressions are generally true.

The equations (35) through (38) must be preserved at the 1-D cell interfaces. For centered schemes the continuities can be enforced by using the same interpolation stencil for the left/right interpolations to the cell interface from the left/right cell centers. This is the method chosen for the GRFFE version of HARM. These constraints on the fields form an implicit constraint on the drift velocity and the magnetic field. Notice that equations (37) and (38) enforce no specific constraint unless there is an enforced surface charge or surface current. Also notice that these constraints must also be preserved in ideal GRMHD.

Interpolating the electric and magnetic field can lead to unphysical interface states if $B^2 - E^2 < 0$ is unconstrained at the interface. To avoid this, one can interpolate $\gamma \tilde{E}_\alpha$ and γ separately and then reconstruct \tilde{E}_α for a given interpolated γ at the interface. This guarantees that the interface state is physical and reasonably similar to the center states.

An alternative scheme can be designed with a staggered grid that automatically enforces these constraints (Del Zanna et al. 2003). However, both methods involve the same number of interpolations since in their case they must interpolate the interface field components to the center before performing the inversion from conserved to primitive quantities. They must also use a stencil that guarantees no discontinuities at their cell center. Thus both methods are equivalent.

2.4 Energy Conservation

The formulation above for the inversion in force-free electrodynamics only explicitly requires T_i^t and not T_t^t , which is a similar feature to other methods (Komissarov 2002b; Krasnopolsky et al. 2005). Since the truncation error in each T_μ^t is independent, the conserved quantity associated with energy conservation (T_t^t) is generally inconsistent with T_i^t . Hence, energy is only conserved to truncation error. As for any numerical scheme that only conserves energy to truncation error, this error can be used to gauge the reliability of the integration. However, in steady-state problems this truncation error may be secular and build-up and lead to unrealistic solutions. It is fruitful to formulate the inversion to

enforce energy conservation and compare the nonconservative integration with a conservative one to gauge the actual effect of the truncation error.

One requires a solution for T_i^t as a function of an arbitrary set of three components of T_μ^t . Then an arbitrary choice can be made to move the truncation error from energy to a momentum. For axisymmetric, stationary spacetimes the natural choice of momenta are the radial and θ momenta. This relationship between T_μ^t that only depends otherwise on B^μ can be obtained from

$$T_\nu^\mu \eta_\mu \eta^\nu = \eta^4 \frac{E^2 + B^2}{2}, \quad (39)$$

where equation (10) also gives that

$$E^2 = \left(\frac{-\eta_\alpha \eta_\beta T_\gamma^\alpha T_\delta^\beta}{B^2 \eta^6} \right) \left(g^{\gamma\delta} - \frac{\eta^\gamma \eta^\delta}{\eta^2} - \frac{B^\gamma B^\delta}{B^2} \right). \quad (40)$$

Equation (40) does not actually depend on T_i^t for our choice of η^μ . Equation (39) gives T_t^t in terms of T_i^t and B^i . Notice that contracting with only η^ν shows that $\eta^\nu T_\nu^\mu$ just reduces to $\eta_\alpha B^\beta T_\beta^\alpha = 0$ for $\nu \neq t$. This shows that of the three T_i^t 's that only two are independent for a fixed B^i . However, for an arbitrary magnetic field, the evolution of all three T_i^t 's is required to avoid singular expressions.

To replace any particular T_i^t with T_t^t , one solves the quadratic equation (39) for that spatial component in terms of T_t^t and the remaining spatial components. This new set of effective T_i^t 's can then be plugged into equation (10). Notice that in general the quadratic equation gives two solutions. This degeneracy is introduced by using the energy, which lacks directional information. In practice it is sufficient to use the solution closest to the one obtained originally from integration of only the spatial parts (T_i^t). This procedure can be used to keep energy and angular momentum conserved to machine error, unlike in prior methods (Komissarov 2002b; Krasnopolsky et al. 2005). Care must be taken for numerical methods with a large truncation error in the energy, since the evolution of the spatial and temporal stress-energy components may be disparate. The origin of this larger truncation error is the larger nonlinearity of the energy compared to the momentums. Lack of energy-momentum conservation can also be due to dissipative processes, as described in the next section.

2.5 Dissipation in Force-Free Electrodynamics

There is no evolutionary constraint in dissipationless force-free electrodynamics that preserves $B^2 - E^2 > 0$, whose violation is taken as evidence that the plasma being modelled would have a nonnegligible inertial back-reaction on the electric field. This typically occurs in current sheets or in regions where the inertia would restrict the field to have a velocity of $v < c$. A physical system responds by dissipating the electric field into other forms of energy.

The dissipation of the electric field is determined by an Ohm's law. For magnetospheres with an ample supply of charges (i.e. not "charge-starved") the Ohm's law in force-free electrodynamics is well-approximated by a large conductivity along the magnetic field and a vanishing conductivity perpendicular to the magnetic field (Komissarov 2004a, 2005b). This reduces Ohm's law to the condition $\mathbf{E} \cdot \mathbf{B} = 0$

and the only perpendicular current is the drift current with velocity given by equation (18).

To model this dissipation, Komissarov (2005b) use the prescription that if $B^2 - E^2 < 0$, then they introduce a large cross-field conductivity. They also have to modify the drift velocity to keep $v < c$. The problem with this prescription is that there is no dissipation until $v > c$. Indeed, in currents sheets the rate of dissipation is related to the drift velocity and is allowed to be $v \rightarrow c$, leading to the fastest possible reconnection rate.

Lyubarsky (2005) study the relativistic Sweet-Parker sheet and Petschek configuration and determine that the rate of reconnection is much less than the speed of light, contrary to previous estimates (see, e.g. Lyutikov 2003; Lyutikov & Uzdensky 2003). This suggests that dissipation should limit the drift of field into a current sheet.

First, inertial losses due to the dissipation of the electric field in a relativistic flow, such as beyond the light cylinder of a rotating compact object, can be “captured” by limiting the Lorentz factor of the drift velocity. This is a similar approach taken in GRMHD numerical models in order to avoid significant numerical errors at large Lorentz factors. A simple prescription is to limit $\gamma \equiv -u^\alpha \eta_\alpha$ such that $1 \leq \gamma^2 \leq \gamma_{max}^2$. From $-1 = u^\alpha u_\alpha$, this means replacing B^2 in equation (18) (and the similar B^2 in the second term of equation 17) with

$$P^2 = \sqrt{\frac{(-\eta^2)E^2 B^2}{1 - \frac{1}{\gamma_{max}^2}}} \quad (41)$$

only when $1 > \gamma^2 > \gamma_{max}^2$. This gives a limited 3-velocity of

$$v^i = -\beta^i + \alpha^2 \frac{[ijk]E_j B_k}{\sqrt{-g}P^2}, \quad (42)$$

that has a continuous transition between standard force-free electrodynamics and dissipative electrodynamics. The 4-velocity given by equation (17) is, by construction, limited to always be time-like and have $\gamma \leq \gamma_{max}$. The energy-momentum lost in such a limiting procedure is assumed to be gained by inertial mass in the form of, e.g., (rapidly lost) thermal or field-aligned kinetic energy that has no effect on the field.

Second, current sheets dissipate due to advection of field into the sheet and subsequent reconnection and cancelation of the magnetic field. Even under exactly symmetric conditions, numerical round-off error quickly leads to random velocity drifts across the current sheet. This magnetic field advection can be limited or avoided by limiting the drift velocity perpendicular to the current sheet. For example, the 3-velocity given by equation (42) can be further modified to have a small or vanishing component perpendicular to the current sheet. That is, if n^i is the spatial normal vector of the current sheet plane at a particular time-slice, then we can set

$$n^j v^i g_{ij} = 0 \quad (43)$$

within some infinitesimal region bounding the current sheet. This changes Ohm’s law in equation (27) to have a vanishing conductivity perpendicular to field lines, i.e. the spatial part of J_\perp^α vanishes such that the “ $\mathbf{E} \times \mathbf{B}$ drift” vanishes along the normal direction of the current sheet. This explicitly avoids significant reconnection by avoiding anomalous numerical

drifts. This is useful in studying systems for which the effect of reconnection is uncertain and the current sheet may be stable. The above prescription can be generalized to set *any* arbitrary drift speed into the current sheet. Thus, physical models of the current sheet and reconnection speed can be included in force-free models as long as inertia plays no other role than in the sheet.

At present this is only implemented for a priori known locations of the current sheet, although a general algorithm should be similar to reconnection-capturing methods (see, e.g., Stone & Pringle 2001). In the tests below that have a current sheet, there are 4 numerical grid zones in a current sheet region that are forced to obey the above condition. This guarantees that the stencil, used by the reconstruction and other dissipative procedures in HARM, does not couple quantities diffusively across the sheet. This also ensures that upon convergence testing that this numerical scheme to avoid reconnection in current sheets plays no role in the results.

This formulation ensures that $B^2 - E^2 > 0$ and that current sheets can be forced to be mostly stable, unlike in Komissarov (2002b); Krasnopolsky et al. (2005) and is improved compared to Komissarov (2005b).

2.6 Quasi-GRMHD and Stationary Force-Free

While this paper describes a GRFFE formulation, since the same code also has a GRMHD formulation, one can imagine hybrid schemes that integrate the decoupled equations of motion in the stiff regime where $b^2/\rho_0 \gg 1$, where ρ_0 is the rest-mass density. All GRMHD numerical schemes have difficulties with this regime, so a decoupled evolution may prove useful for studying the first nonzero order effect of inertia in a force-free field. This hybrid method will be used in future work, but the method is outlined here.

In the force-free limit, one may still retain the evolution of the rest-mass and internal energy density with no back reaction onto the field (see also Mestel & Shibata 1994; Contopoulos 1995; Contopoulos et al. 1999). The method is to evolve the full GRMHD equations of motion, but to determine the field-perpendicular velocity components and field from the force-free equations alone. In this case one can readily obtain the field-aligned velocity component from the GRMHD inversion. That is, in ideal GRMHD in general, the fluid velocity may be broken into a field-perpendicular and a field-aligned velocity or equivalently into an electromagnetic and a matter velocity,

$$u_{FL}^\alpha = u_\perp^\alpha + u_\parallel^\alpha = u_{EM}^\alpha + u_{MA}^\alpha. \quad (44)$$

Also of interest is the fluid motion in a stationary force-free field, which allows a study of the Lorentz factor along a force-free field line (Mestel & Shibata 1994; Contopoulos 1995; Contopoulos et al. 1999). For an stationary, axisymmetric model the energy (Bernoulli) equation alone determines the field-aligned velocity and the frozen-in conditions,

$$\frac{u_{FL}^r}{B^r} = \frac{u_{FL}^\theta}{B^\theta} = \frac{u_{FL}^\phi - \Omega_F u_{FL}^t}{B^\phi}, \quad (45)$$

apply to the fluid velocity and by $u_\alpha^{EM} B^\alpha = 0$,

$$\frac{u_{EM}^r}{B^r} = \frac{u_{EM}^\theta}{B^\theta} = \frac{u_{EM}^\phi - \Omega_F u_{EM}^t}{B^\phi}, \quad (46)$$

apply to the electromagnetic velocity. These equations can be solved for the electromagnetic 3-velocity to obtain

$$v_{EM}^i = \Omega_F \phi^i - B^i B_\mu \left(\frac{t^\mu + \Omega_F \phi^\mu}{B^2} \right) \quad (47)$$

where t^μ and ϕ^μ are the time and ϕ Killing vectors and $B_\mu = g_{\mu\nu} B^\nu$. That is, for stationary, axisymmetric solutions the magnetic field and Ω_F alone determine the electromagnetic velocity, unlike in general as given by equation (18).

3 ALGORITHM TESTS

A parameter space test of the analytic GRFFE inversion described above was performed to evaluate the range of allowed Lorentz factors the inversion is capable of handling. The procedure is to start with a known v^i and B^i for a specific point in space-time, determine T_μ^t , and then invert to get v^i . Double precision is used for all quantities. The typical failure mode is that the velocity is determined to be space-like, and this is nearly coincident with a significant increase in the error in the inversion. Of interest is the general maximum value of the Lorentz factor below which no failures occur.

In Minkowski space-time tests, the maximum Lorentz factor is $u^t \sim 10^{10}$ before roundoff error causes the inversion to suddenly have significant error. Below this u^t , the relative error is similar to machine error. As an extreme test, the space-time point is chosen in Kerr-Schild coordinates with a Kerr spin parameter of $a/M = 0.9375$ for a point on the horizon at $\theta = \pi/4$. For grid-aligned flows the maximum Lorentz factor is $u^t \sim 10^{10}$ as before. However, for arbitrary flow directions, the inversion can fail for $u^t \gtrsim 2200$. Most astrophysical flows of interest have $u^t < 2000$, so this is sufficient for our purposes. Otherwise a smaller machine precision should be used.

The GRFFE formulation is coupled to HARM to test the formulation's ability to handle typical force-free problems. The GRFFE formulation is used in HARM to perform the Minkowski space-time test calculations that are described by Komissarov (2002b, 2004a). These tests include: 1) a fast wave ; 2) a degenerate Alfvén wave ; 3) a three-wave problem ; 4) a problem that evolves to $B^2 - E^2 < 0$; 5) a standing Alfvén wave ; and 6) two current sheet problems. Since our GRFFE formulation assumes $\mathbf{E} \cdot \mathbf{B} = 0$, their non-degenerate Alfvén wave test is not considered.

Their notation of the “wave frame” fields E' and B' are equivalent to the HARM notation for $e^\mu = 0$ and b^μ for $E' = 0$, and otherwise the wave frame, E' , and B' can be processed through the inversion routine to setup an initial lab-frame B^i and v^i from their E' , B' , and speed μ . The other problems they setup only require the lab-frame E and B , and again our GRFFE inversion can be used to obtain the initial lab-frame B^i and v^i as long as the problem is degenerate. Note that our sign conventions for E and B agree with theirs. We estimate that they used about 200 grid zones for their tests and so use the same number for our tests. We use the same final time, box size, and plot labels for easy comparisons. We shift the $x = 0$ position to be similar for each set of tests in Komissarov (2002b, 2004a). A Courant factor of 0.9 and the monotonized central limiter

is used for all tests except an additional current sheet test with parabolic spatial interpolation.

Notice that apart from the initial condition given in Komissarov (2002b, 2004a), for the fast wave one requires a relation determined earlier in their paper: $E^z = C - \mu_f B^y$, where C is constrained such that $B^2 - E^2 < 0$ ($C = 1$ was chosen) and $\mu_f = +1$ was chosen by them.

Figure 1 shows the suite of tests demonstrated in Komissarov (2002b). For the top 3 panels, the solid line denotes the analytic solution at the initial and final time. The diamonds denote the numerical solution at the final time. The top panel shows B_2 for the fast wave. The head of the wave is more resolved than in Komissarov (2002b), but the tail of the wave is slightly less resolved. The second and third panels from the top show B_2 and B_3 for the degenerate Alfvén wave problem. The code does well to capture both fast and Alfvén waves. The next two panels show B_2 and E_1 for the three-wave problem. The waves are resolved similarly as in Komissarov (2002b). The bottom panel shows $b^2/B^2 = (B^2 - E^2)/B^2$ for the smoothed $B^2 - E^2 \rightarrow 0$ test problem. Overall, the GRFFE version of HARM performs comparably to the code by Komissarov (2002b) based on more complicated Riemann solvers.

Figure 2 shows the suite of tests demonstrated in Komissarov (2004a). The top panel shows B_z for a stationary Alfvén wave. This wave is much more resolved than in Komissarov (2004a) and indicates that the code's effective resistive diffusion coefficient is quite low. The next panel shows E_z and B_y for a current sheet problem as described in Komissarov (2004a) with $B_0 = 0.5$. The features are well-resolved. The two bottom panels show the second current sheet problem with $B_0 = 2$. The upper of the two is using the MC limiter, while the lower of the two is using a parabolic interpolation (Colella 1984), which gives similar results to Komissarov (2004a). In the fast wave region the MC limiter gives a Lorentz factor of $\Gamma = 1.90$, while the parabolic method gives $\Gamma = 2000$, the largest allowed Lorentz factor. For either method, the region at $x^1 = 0.5$ within the current sheet reaches $B^2 - E^2 \sim 0$, but the Lorentz factor limiter (here limited to $\gamma_{max} = 2000$) keeps the code stable despite the presence of the current sheet. No complicated dissipation model had to be included to achieve such a result.

4 PHYSICAL MODELS

This section considers astrophysical models for which the GRFFE approximation is a reasonable one. The GRFFE formulation is used in HARM.

Komissarov (2004a) study the Wald (Wald 1974) and split-monopole BZ77 (Blandford & Znajek 1977) solutions for slowly and moderately rapidly rotating black holes. Of particular interest is whether the Wald and split-monopole solutions can be better represented compared to as shown in figures 3 and 4 of Komissarov (2004a). We consider the monopole and split-monopole for slowly rotating black holes in this paper.

The other models are considered in a separate paper (McKinney 2005e), which demonstrates our GRFFE formulation's ability to handle the current sheet in the actual *split-monopole* solution of Blandford & Znajek (1977) and the Wald problem with a rapidly rotating black hole spin. In

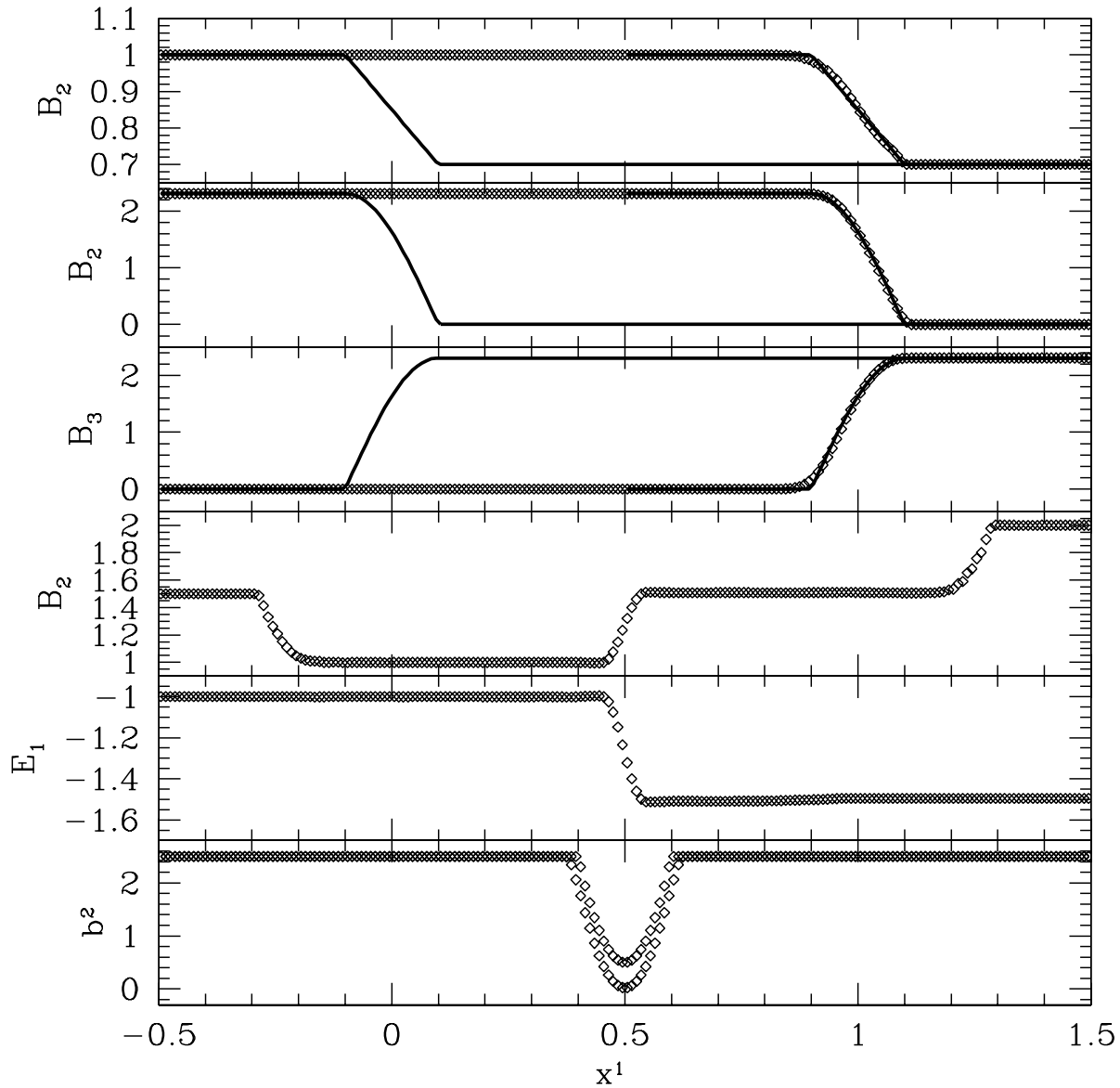


Figure 1. Suite of tests described by Komissarov (2002b). Solid curves represent the initial and final analytic solution for the top three panels. Diamonds represent the numerical solution at the final time, except for the plot of b^2 that shows both times. Tests are as follows from top to bottom: 1) B_2 for fast wave ; 2) B_2 and B_3 for degenerate Alfvén wave ; 3) B_2 and E_1 for three-wave problem ; and 4) initial and final smoothed $b^2 = B^2 - E^2 \rightarrow 0$ problem.

that paper for the Wald problem, we were able to reach similar solutions Komissarov (2005a) who used an MHD model to avoid significant reconnection in the current sheet that developed in their force-free models Komissarov (2004a).

Neutron star magnetospheres are studied in a separate paper (McKinney 2005d), which demonstrates that the GRFFE code can be used to study pulsar magnetospheres even in the presence of a current sheet. That paper shows we are able to avoid the problems encountered by Komissarov (2005b) with force-free and the current sheet. We found similar results to, but more accurate than, their ideal MHD results.

In this paper we focus on slowly rotating black hole magnetospheres that require general relativity and so full GRFFE. The interesting quantities that are plotted throughout the following sections are $\Omega_F \equiv F_{t\theta}/F_{\theta\phi}$, which is also $\Omega_F = F_{tr}/F_{r\phi}$ for a stationary, axisymmetric flow. This quantity often appears as a ratio to the black hole angular velocity of $\Omega_H \equiv a/(2r_+)$. The radial and θ magnetic field strengths for these plots is defined as in Komissarov (2004a), with $B^i \equiv {}^*F^{it}$. Also interesting is the conserved

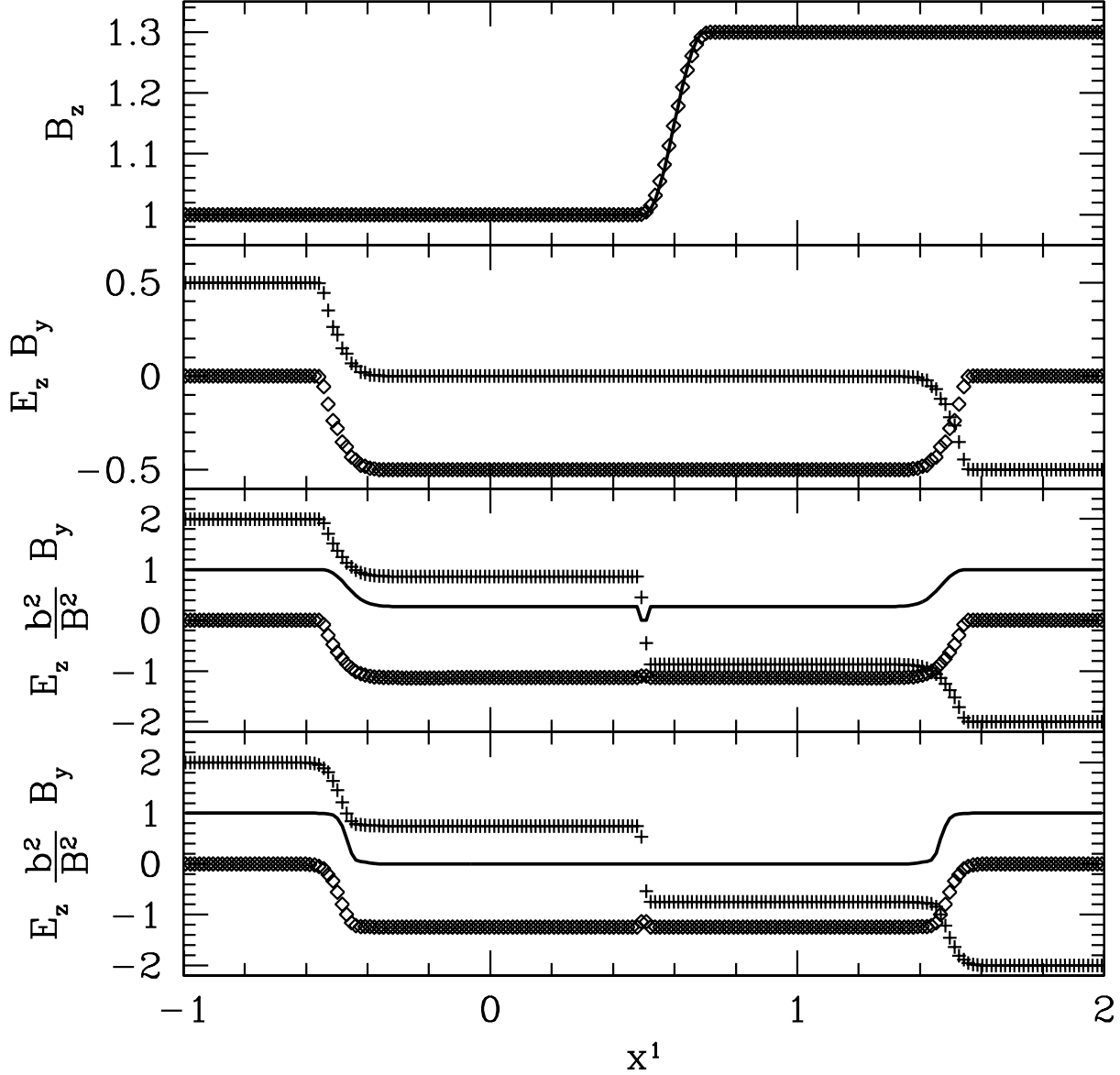


Figure 2. Suite of tests described by Komissarov (2004a). Solid curves represent the initial and final analytic solution except in the bottom panel. Pluses and diamonds represent the numerical solution at the final time. Tests are as follows from top to bottom: 1) B_z for stationary Alfvén wave ; 2) E_z and B_y for current sheet with $B_0 = 0.5$; 3,4) E_z , b^2 , and B_y for current sheet with $B_0 = 2$. Third is with 2nd order method and fourth is with 4th order method.

toroidal flux of $\sqrt{-g}\tilde{B}_\phi \equiv B_\phi \equiv {}^*F_{t\phi} = \sqrt{-g}F^{r\theta}$.¹ This is because the electromagnetic energy flux is $F_E^i = -T_t^i = -B^i\Omega_F B_\phi$ and the electromagnetic angular momentum flux is $F_L^i = F_E^i/\Omega_F$. Also of interest is the magnetic vector potential (A_ϕ), whose contours are plotted and represent flow surfaces. For axisymmetric, stationary flows these surfaces define surfaces of constant Ω_F , B_ϕ , F_E^i/B^i , and F_L^i/B^i in dissipationless force-free electrodynamics. Finally, also of interest are the light surfaces, which are defined for the case

¹ Notice the slight change, for simplicity, in notation for B_ϕ and B^i from this point onward.

of a purely rotational velocity $\Omega = \Omega_F$ leads to a null trajectory, i.e. from $u^\alpha u_\alpha = -1$,

$$g_{tt} + 2\Omega g_{\phi t} + \Omega^2 g_{\phi\phi} = 0. \quad (48)$$

4.1 Black Hole Magnetosphere: Blandford-Znajek Monopole and Split-Monopole

Komissarov (2002b) demonstrated the stability of the *pure* monopole solution of Blandford & Znajek (1977) by studying one hemisphere. Our GRFFE formulation generates quantitatively similar results. Krasnopolsky et al. (2005) also use a method based on HARM and study the depen-

dence of the field (purely monopolar-type) geometry and field rotation frequency on black hole spin. They also studied how the energy output varies with black hole spin up to $a/M = 0.9999$. They find that the energy output follows $\dot{E} \propto \Omega_H^2$ up to $a/M = 0.98$. This is in contrast to the energy output in the presence of a thick disk that follows $\dot{E} \propto \Omega_H^3 \propto \Omega_F^3$ when accounting for the mass accretion rate (McKinney 2005a). This suggests that the presence of matter can be important. However, there may be systems that are dominated by a magnetosphere rather than a disk (see, e.g., Igumenshchev et al. 2003; Narayan et al. 2003). For such systems, the force-free limit may be sufficient to describe the energetics and geometry of the field lines.

For the purposes of testing, the pure monopole Blandford-Znajek solution is considered, as in section 5.2 of Komissarov (2004a). An identical numerical setup to Komissarov (2004a) is used. A grid is chosen with an outer radius of $r = 260GM/c^2$. There are 150 equally-logarithmically-spaced radial zones and 100 uniform θ zones. As mentioned in Komissarov (2004a), the final result is insensitive to the details of the initial conditions, so the simple $a/M = 0$ monopole solution is chosen as an initial condition. The evolution proceeds until $t = 50GM/c^3$.

Figure 3 shows Ω_F/Ω_H (top panel), $-B_\phi$ (middle panel; pluses), analytic Blandford-Znajek (BZ) solution for $-B_\phi$ (middle panel; solid line), $-B^r/10$ (middle panel; short dashed line), B^θ (middle panel; long dashed line), and $\mathbf{E} \cdot \mathbf{B}$ for $\theta = \pi - 0.1$ and $\theta = 0.1$. The figure is directly comparable to figure 2 in Komissarov (2004a). The value of Ω_F/Ω_H only varies monotonically from 0.5013 near the equator to 0.5009 at the poles. Unlike in Komissarov (2004a), the value does not rise again near the poles, which suggests HARM is properly resolving the coordinate singularity. Their value is up to 0.503 near the equator, which suggest HARM is doing marginally better. The middle panels shows that the code is very accurately reproducing the BZ solution. The solid line indicating the analytic solution is not visibly deviating from the crosses that mark the numerical solution. The bottom panel just advertises the fact that HARM is uniformly preserving $\mathbf{E} \cdot \mathbf{B} = 0$ to machine precision, where figure 2 in Komissarov (2004a) shows nonuniform errors of order 10^{-4} .

Komissarov (2004a) study the Wald and split-monopole BZ77 solution for slowly and moderately rapidly rotating black holes. Of particular interest is whether the Wald and split-monopole solutions can be better represented compared to as shown in figures 3 and 4 of Komissarov (2004a). This paper demonstrates our GRFFE formulation’s ability to handle the current sheet in the actual *split*-monopole solution of Blandford & Znajek (1977).

We use an identical setup to Komissarov (2004a) for the split-monopole case with a black hole with spin $a = 0.1^2$. There are 100 uniform θ zones with 80 radial zones such that $dr/r = \text{Const.}$. The model is axisymmetric and the inner boundary is placed inside the horizon and the outer boundary is at $r = 29GM/c^2$. The model is run till $t = 5GM/c^3$ as in Komissarov (2004a).

² Komissarov (2004a) pointed out in their section 5.3 that $a = 0.1$, but then their figure 3 caption says “Schwarzschild”. The $a = 0$ and $a = 0.1$ models show the same results, so this issue is not crucial.

Figure 4 shows a two panel plot that can be directly compared with figure 3 in Komissarov (2004a). In their model the current sheet rapidly reconnects even over this very short time period. Our results show essentially zero reconnection. This is primarily due to the modifications of the drift velocity described in section 2.5, and secondarily due to the low diffusivity of the algorithm as demonstrated in section 3. Without the drift velocity modification, however, our results are similar to shown in figure 3 of Komissarov (2004a). So this demonstrates the usefulness of the relatively ad hoc approach of treating current sheets.

For this model, we used the local Lax-Friedrich (LLXF), rather than the Harten-Lax-van Leer (HLL), approximate nonlinear Riemann solver (see, e.g. Gammie et al. 2003a). The HLL solver generated fluctuations at the inner-radial boundary that back propagate through the horizon due to numerical diffusion. HLL is explicitly causal. However, in HARM and all numerical methods the author is aware of (for an exception see, e.g. Hawke et al. 2005), the stencil used to reconstruct the quantities to the Riemann interface is still acausal. For example, in HARM, the stencil is always centered and so connects information across the horizon depending upon the smoothness of the flow. The author knows of no numerical method that accounts for the characteristic information in constraining the reconstruction to be causal. In McKinney (2005e), we consider modifications to the stencil that enforce strict causality. This eliminates all the problems described above.

5 CONCLUSIONS

We described a GRFFE formulation that allows GRMHD codes to directly evolve the GRFFE equations of motion. Rather than evolving the electric and magnetic fields, the velocity and magnetic field are directly evolved. This formulation strictly enforces $\mathbf{E} \cdot \mathbf{B} = 0$, $\nabla \cdot \mathbf{B} = 0$, and energy conservation, unlike prior codes. Established, accurate, and well-tested GRMHD codes can simply add a new inversion piece of code to their existing code, while continuing to use all the already-developed facilities present.

We also introduced a simplified general model of the dissipation of the electric field to enforce the $B^2 - E^2 > 0$ constraint. This limits the code to a regime of Lorentz factors that the code can handle without significant numerical errors.

A simplified general model was introduced to allow current sheets to be resolved, without reconnection, over many dynamical times. The other improvements to the code, such as strict enforcement of $\mathbf{E} \cdot \mathbf{B} = 0$, $\nabla \cdot \mathbf{B} = 0$, energy conservation, and $B^2 - E^2 > 0$ do not play a role in this improvement. Limiting the numerically induced drift velocity perpendicular to the sheet was a crucial step to make such a force-free code useful, and resolves the difficulties encountered by prior authors (Komissarov 2004a, 2005b). For highly magnetized systems, our GRFFE results are as good as ideal MHD results without the need to introduce an artificial evolution of the rest-mass and internal energy densities. Evidence of this fact is shown in other papers (McKinney 2005d,e), where we model particular astrophysical systems.

Numerical tests showed that the GRFFE formulation as used in HARM is robust and accurate. HARM uses

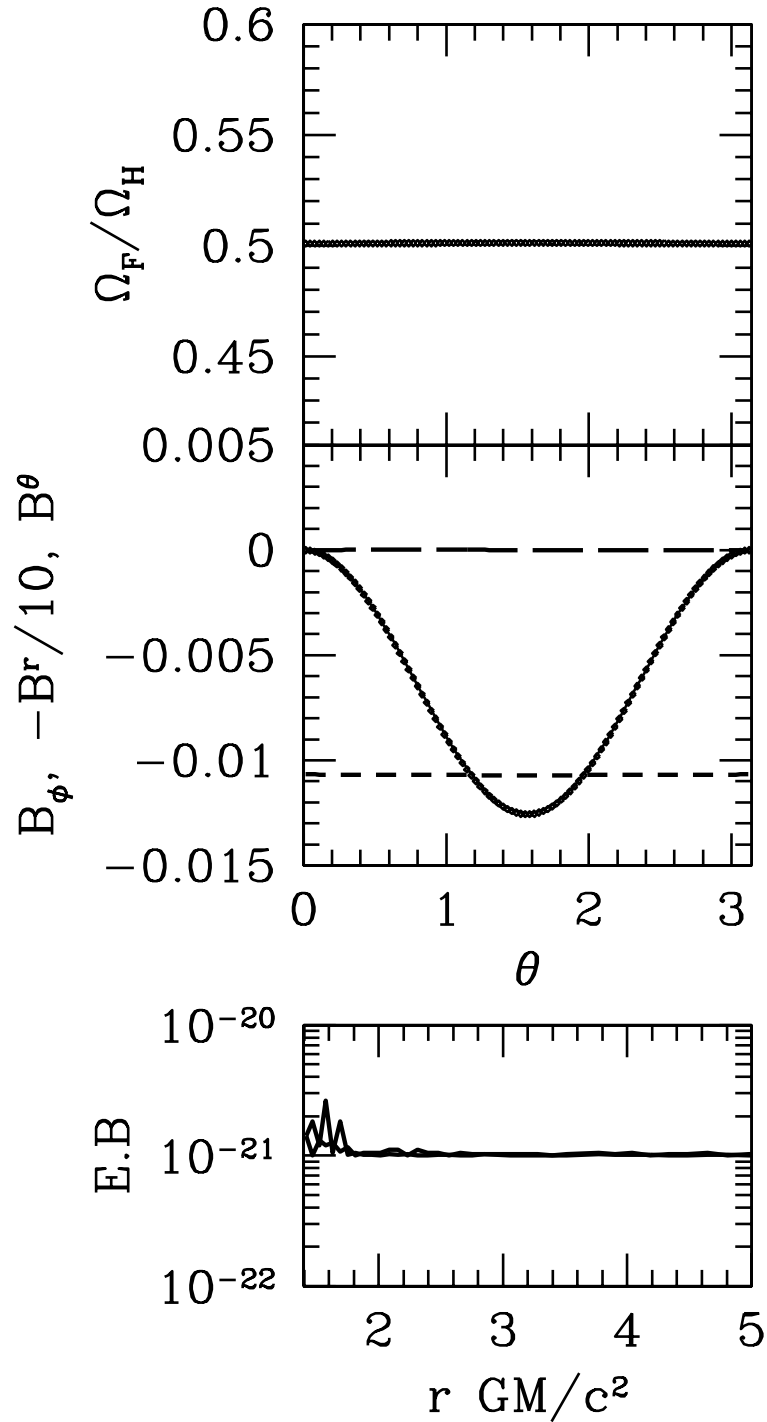


Figure 3. Pure monopole Blandford-Znajek solution for black hole spin $a/M = 0.1$. Upper panel: Ω_F/Ω_H . Middle panel: $-B_\phi$ (dotted: numerical, solid: analytic), B^r (short dashed), and B^θ (long dashed). Lower panel: $\mathbf{E} \cdot \mathbf{B}$. Model at $t = 50GM/c^3$. Directly comparable with figure 2 in Komissarov (2004a).

a simplified nonlinear approximate Riemann solver as in Krasnopolsky et al. (2005), which, while being much simpler than the exact Riemann solution by Komissarov (2002b), produced as accurate results.

For the pure monopole Blandford-Znajek model, we found similar results as Komissarov (2002b); Krasnopolsky et al. (2005). We also demonstrated our

code's ability to handle current sheets, which was found to be difficult in Komissarov (2004a). Here and in McKinney (2005e), the split-monopole problem was able to be solved without significant reconnection. This allows one to study general magnetospheres with arbitrary currents in a sheet, such as the paraboloidal field. McKinney (2005e) also discusses the Wald solution, and it shows that our code is able

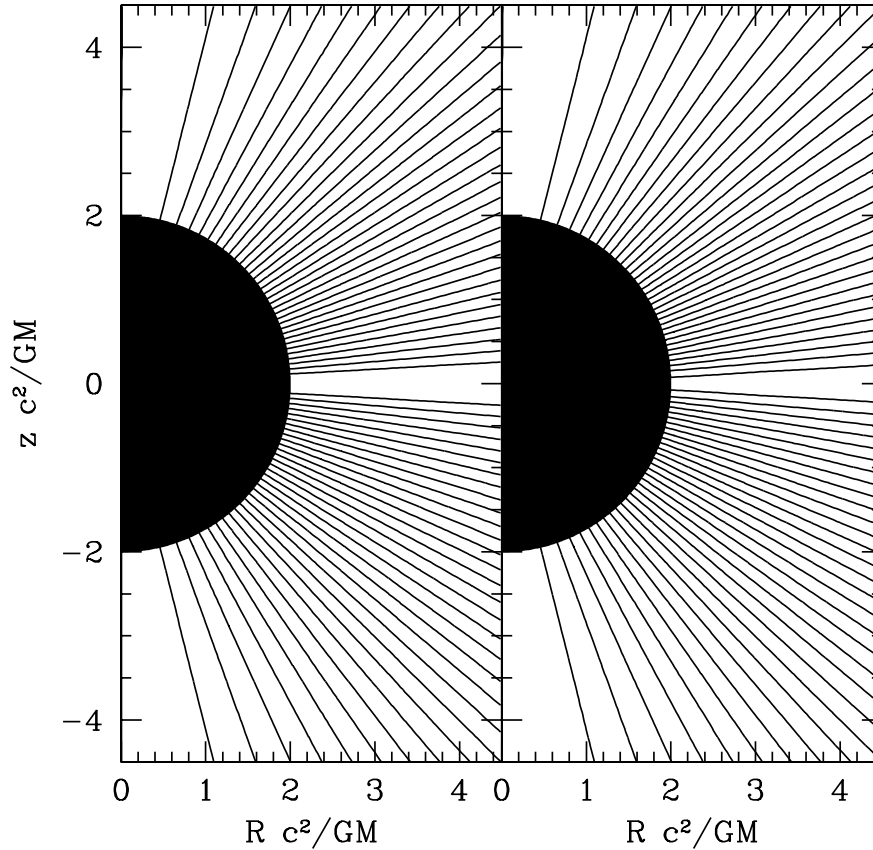


Figure 4. Contours of the magnetic vector potential component A_ϕ , giving the field lines for the split-monopole Blandford-Znajek solution for black hole spin $a/M = 0.1$. Left panel: Initial Model. Right panel: Model at $t = 5GM/c^3$. Directly comparable with figure 3 in Komissarov (2004a).

to obtain similar results as the MHD code of Komissarov (2005a), while Komissarov (2004a) encountered difficulties with the current sheet reconnecting too fast.

ACKNOWLEDGMENTS

This research was supported by NASA-Astrophysics Theory Program grant NAG5-10780 and a Harvard CfA Institute for Theory and Computation fellowship. I thank Alexandre Tchekhovskoi and Avery Broderick for useful discussions that pushed the project forward. I thank Ian Morrison, Ruben Krasnopolsky, and Charles Gammie for discussions regarding the original simplified HARM-like GRFFE formulation during my time with them at the UIUC. I thank Serguei Komissarov and Dmitri Uzdensky for comments.

REFERENCES

- Anile, A.M. 1989, *Relativistic Fluids and Magneto-fluids*, (New York: Cambridge Univ. Press)
- Anninos, P., Fragile, P. C., & Salmonson, J. D. 2005, *ArXiv Astrophysics e-prints*, arXiv:astro-ph/0509254
- Anton, L., Zanotti, O., Miralles, J. A., Marti, J. M., Ibanez, J. M., Font, J. A., & Pons, J. A. 2005, *ArXiv Astrophysics e-prints*, arXiv:astro-ph/0506063
- Baumgarte, T. W., & Shapiro, S. L. 2003, *ApJ*, 585, 921
- Begelman, M. C., & Li, Z. 1994, *ApJ*, 426, 269
- Begelman, M. C. 1998, *ApJ*, 493, 291
- Beskin, V. S., & Nokhrina, E. E. 2005, *ArXiv Astrophysics e-prints*, arXiv:astro-ph/0506333
- Blandford, R. D. & Znajek, R. L. 1977, *MNRAS*, 179, 433
- Colella, P., & Woodward, P., 1984, *JCP*, 54, 174
- Contopoulos, J. 1995, *ApJ*, 446, 67
- Contopoulos, I., Kazanas, D., & Fendt, C. 1999, *ApJ*, 511, 351
- Del Zanna, L., Bucciantini, N., & Londrillo, P. 2003, *A&A*, 400, 397
- De Villiers, J.-P., & Hawley, J. F. 2003, *ApJ*, 589, 458
- Duez, M. D., Liu, Y. T., Shapiro, S. L., & Stephens, B. C. 2005, *Phys. Rev. D*, 72, 024028
- Gammie, C. F., McKinney, J. C., & Gábor Tóth 2003, *ApJ*, 589, 444
- Gammie, C. F., Shapiro, S. L., & McKinney, J. C. 2004, *ApJ*, 602, 312
- Goldreich, P., & Julian, W. H. 1969, *ApJ*, 157, 869

- Goodwin, S. P., Mestel, J., Mestel, L., & Wright, G. A. E. 2004, *MNRAS*, 349, 213
- Gruzinov, A. 2005, *Physical Review Letters*, 94, 021101
- Hawke, I., Löffler, F., & Nerozzi, A. 2005, *Phys. Rev. D*, 71, 104006
- Igumenshchev, I. V., Narayan, R., & Abramowicz, M. A. 2003, *ApJ*, 592, 1042
- Koide, S., Shibata, K., & Kudoh, T. 1999, *ApJ*, 522, 727
- Komissarov, S. S. 1999, *MNRAS*, 303, 343
- Komissarov, S. S. 2001, *MNRAS*, 326, L41
- Komissarov, S. S. 2002a, *ArXiv Astrophysics e-prints*, arXiv:astro-ph/0211141
- Komissarov, S. S. 2002b, *MNRAS*, 336, 759
- Komissarov, S. S. 2004a, *MNRAS*, 350, 427
- Komissarov, S. S. 2004b, *MNRAS*, 350, 1431
- Komissarov, S. S. 2005a, *MNRAS*, 359, 801
- Komissarov, S. S. 2005b, *ArXiv Astrophysics e-prints*, arXiv:astro-ph/0510310
- Krasnopolsky, R., Morrison, I., Gammie, C.F. 2005, in prep.
- Li, L. 2000, *ApJ*, 531, L111
- Lichnerowicz, A. 1967, *Relativistic Hydrodynamics and Magnetohydrodynamics*, New York: Benjamin, 1967
- Lichnerowicz, A. 1976, *Journal of Mathematical Physics*, 17, 2135
- Lyubarsky, Y. E. 2005, *MNRAS*, 358, 113
- Lyutikov, M., & Blandford, R. 2003, *ArXiv Astrophysics e-prints*, arXiv:astro-ph/0312347
- Lyutikov, M. 2003, *MNRAS*, 346, 540
- Lyutikov, M., & Uzdensky, D. 2003, *ApJ*, 589, 893
- McKinney, J. C., & Gammie, C. F. 2004, *ApJ*, 611, 977
- McKinney, J. C. 2005a, *ApJ*, 630, L5
- McKinney, J. C. 2005b, *ArXiv Astrophysics e-prints*, arXiv:astro-ph/0506369
- McKinney, J. C. 2005c, *ArXiv Astrophysics e-prints*, arXiv:astro-ph/0506368
- McKinney, J. C. 2005d, *ArXiv Astrophysics e-prints*, arXiv:astro-ph/0601411
- McKinney, J. C. 2005e, *ArXiv Astrophysics e-prints*, arXiv:astro-ph/06xxxxx
- Mestel, L., & Shibata, S. 1994, *MNRAS*, 271, 621
- Misner, C. W., Thorne, K. S., & Wheeler, J. A. 1973, *San Francisco: W.H. Freeman and Co.*, 1973,
- Narayan, R., Igumenshchev, I. V., & Abramowicz, M. A. 2003, *PASJ*, 55, L69
- Okamoto, I. 1999, *MNRAS*, 307, 253
- Okamoto, I. 2000, *MNRAS*,
- Okamoto, I. 2003, *ApJ*, 589, 671
- Shibata, M., & Sekiguchi, Y.-I. 2005, *Phys. Rev. D*, 72, 044014
- Spruit, H. 1996, in *Evolutionary Processes in Binary Stars*, NATO ASI Series C., 477, 249 (astro-ph/9602022)
- Stone, J. M. & Pringle, J. E. 2001, *MNRAS*, 322, 461
- Tomimatsu, A., Matsuoka, T., & Takahashi, M. 2001, *Phys. Rev. D*, 64, 123003
- Toro, E. F., 1999, *New York: Springer-Verlag, Second Edition*, 1999
- Wald, R. M. 1974, *Phys. Rev. D*, 10, 1680